The Astrophysical Journal, 640:308–318, 2006 March 20

INTERFEROMETRIC MEASUREMENTS OF VARIABLE 340 GHz LINEAR POLARIZATION IN SAGITTARIUS A*

Daniel P. Marrone, James M. Moran, Jun-Hui Zhao, and Ramprasad Rao[1]
Harvard-Smithsonian Center for Astrophysics, 60 Garden Street, Cambridge, MA 02138; dmarrone@cfa.harvard.edu
Received 2005 September 6; accepted 2005 November 21

ABSTRACT

Using the Submillimeter Array, we have made the first high angular resolution measurements of the linear polarization of Sagittarius A* at submillimeter wavelengths and the first detection of intraday variability in its linear polarization. We detected linear polarization at 340 GHz (880 μm) at several epochs. At the typical resolution of $1\farcs4 \times 2\farcs2$, the expected contamination from the surrounding (partially polarized) dust emission is negligible. We found that both the polarization fraction and the position angle are variable, with the polarization fraction dropping from 8.5% to 2.3% over 3 days. This is the first significant measurement of variability in the linear polarization fraction in this source. We also found variability in the polarization and total intensity within single nights, although the relationship between the two is not clear from these data. The simultaneous 332 and 342 GHz position angles are the same, setting a 1 σ rotation measure (RM) upper limit of 7×10^5 rad m^{-2}. From position angle variations and comparison of "quiescent" position angles observed here and at 230 GHz, we infer that the RM is a few times 10^5 rad m^{-2}, a factor of a few below our direct detection limit. A generalized model of the RM produced in the accretion flow suggests that the accretion rate at small radii must be low, below 10^{-6}–10^{-7} $M_\odot$ yr^{-1} depending on the radial density and temperature profiles, but in all cases below the gas capture rate inferred from X-ray observations.

Subject headings: black hole physics — Galaxy: center — instrumentation: polarimeters — polarization — submillimeter — techniques: interferometric

1. INTRODUCTION

The radio source Sagittarius A* (Sgr A*) has been conclusively identified in the radio and infrared with a black hole of mass $\sim 3.5 \times 10^6$ $M_\odot$ at the center of our Galaxy (Reid & Brunthaler 2004; Schödel et al. 2003; Ghez et al. 2005; Eisenhauer et al. 2005). Sgr A* is the nearest supermassive black hole, 100 times closer than its nearest neighbor, M31*, and therefore should provide a unique opportunity to understand the physics and life cycle of these objects. For a black hole of its size, Sgr A* is extremely underluminous, only a few hundred solar luminosities and $10^{-8} L_{\rm Edd}$. This surprisingly low luminosity has motivated many theoretical and observational efforts to understand the processes at work very near to Sgr A*.

Accretion models of Sgr A* generally seek to explain its faintness through inefficient radiative and accretion processes. A variety of physical mechanisms can be invoked to suppress accretion and radiation, including convection (Quataert & Gruzinov 2000a), jets (Falcke et al. 1993), advection of energy stored in nonradiating ions (Narayan & Yi 1994), and winds (Blandford & Begelman 1999). Many models incorporating combinations of these and other phenomena are able to account for the spectrum and low luminosity of Sgr A*. Therefore, the physics of this source are not well constrained by these observations alone.

In recent years, millimeter and submillimeter polarimetry has emerged as an important tool for studies of Sgr A*. Linear polarization and its variability can be used to understand the structure of the magnetic field in the emission region and turbulence in the accretion flow, and possibly to constrain the mechanisms responsible for the multiwavelength variability of this source. Through Faraday rotation of the linear polarization, we can examine the density and magnetic field distributions along the line of sight, and eventually, in the context of more comprehensive models of the accretion flow structure, infer an accretion rate at the inner regions of the accretion flow (Quataert & Gruzinov 2000b; Agol 2000; Melia et al. 2000).

Previous observations of the linear polarization of Sgr A* have found low ($<1\%$) upper limits at 22, 43, and 86 GHz (Bower et al. 1999b), with a 2% limit at 112 GHz (Bower et al. 2001). The lowest frequency detection of linear polarization is at 150 GHz (Aitken et al. 2000), suggesting that these polarimetric probes of Sgr A* can only be exploited at short millimeter and submillimeter wavelengths. Aitken et al. (2000) found that the polarization fraction rises steeply from 150 to 400 GHz, although these observations were made with a single-aperture instrument and therefore required careful removal of contaminant emission within the telescope beam. The steep spectrum and a jump in the polarization position angle between 230 and 350 GHz in the Aitken et al. (2000) data have been taken as evidence of a transition to optically thin synchrotron emission (e.g., Aitken et al. 2000; Agol 2000; Melia et al. 2000). Subsequent interferometric monitoring of the 230 GHz polarization, with angular resolution sufficient to avoid contamination from the surrounding emission, has shown that the 230 GHz polarization fraction appears to remain constant over 5 yr, despite variations in the position angle on timescales of months to years (Bower et al. 2003, 2005). This variability reduces the significance of the observed position angle jump and demonstrates the need for contemporaneous measurements at multiple frequencies. Bower et al. (2005) attribute the variations in the 230 GHz polarization to changes of a few times 10^5 rad m^{-2} in the rotation measure (RM), probably in the accretion medium, rather than to changes in the intrinsic source polarization. As of yet, no observations have been able to determine the RM, but they can place upper limits on the magnitude of the RM and infer temporal variations that are within a factor of a few of the upper limits.

Circular polarization has also been detected in this source, with a rising polarization fraction from 1.4 to 15 GHz (Bower

[1] Current address: Institute of Astronomy and Astrophysics, Academia Sinica, P.O. Box 23-141, Taipei 10617, Taiwan.

et al. 1999a; Sault & Macquart 1999; Bower et al. 2002). Some models seeking to explain the millimeter/submillimeter linear polarization have also predicted appreciable circular polarization at these high frequencies due to the conversion of linear to circular polarization in a turbulent jet (Beckert & Falcke 2002; Beckert 2003). However, measurements to date that are at or above 100 GHz (e.g., Tsuboi et al. 2003; Bower et al. 2003, 2005) have not shown circular polarization at the percent level.

The Submillimeter Array (SMA) has the potential to contribute many new capabilities to these studies. It provides the first opportunity to measure the polarization above 230 GHz at an angular resolution sufficient to separate Sgr A* from its surroundings. Its large bandwidth (2 GHz per sideband), low latitude, and dry site make it far more sensitive for studies of this southern source than the 230 GHz observations of Bower et al. (2003, 2005), which were made with the Berkeley-Illinois-Maryland Association array at Hat Creek, California. Given the sensitivity and the large (10 GHz) sideband separation, 340 GHz polarimetry with the SMA should improve limits on the RM, and future 230 GHz polarimetry may measure it directly. These advantages also apply to measurements of variability in total intensity and polarization and of circular polarization. Here we present the first high angular resolution observations of the submillimeter polarization of Sgr A*, using the newly dedicated SMA and its polarimetry system. We discuss our observations and data reduction in § 2, the data and their relation to previous polarimetry in this source in § 3, and the implications of these new results in § 4. We offer concluding remarks in § 5.

2. OBSERVATIONS

Sgr A* was observed on several nights in 2004 using the Submillimeter Array[2] (Blundell 2004; Ho et al. 2004). The observing dates, zenith opacity, number of antennas used in the reduction, and on-source time are given in Table 1. The local oscillators were tuned to a frequency of 336.7 GHz, centering the 2 GHz wide upper and lower sidebands (USB and LSB) on 341.7 and 331.7 GHz, respectively. This frequency choice avoided strong spectral lines and provided a reasonable match to the frequency response of the SMA polarimetry hardware, as discussed below. Our Sgr A* tracks generally included source elevations between 20° and 41° (transit), a period of 7 hr, although weather, calibration, and technical problems caused variations in the coverage. In the SMA "Compact-North" configuration we sampled projected baselines between 8 and 135 kλ. The average synthesized beam was approximately $1\farcs4 \times 2\farcs2$. According to the estimate in Aitken et al. (2000), polarized emission within the 14″ beam of the James Clerk Maxwell Telescope (JCMT) at 350 GHz contributes 100 mJy of polarized flux density. With a beam smaller by a factor of 60 and reduced sensitivity to large-scale emission, we expect that this contaminant will be negligible in our data.

Each SMA antenna was equipped with a single linearly polarized (LP) feed in each of its three observing bands. Ideally, interferometric observations of linear polarization are made with dual circularly polarized (CP) feeds, as they separate the total intensity (Stokes I) from the linear polarization Stokes parameters (Q and U). For polarimetry we have converted the 340 GHz LP feeds to left- and right-hand circularly polarized (LCP and RCP) feeds using positionable quartz and sapphire quarter-wave plates. The polarization handedness was selected by switching the angular position of the wave plate crystal axes between two positions at ±45° from the polarization angle of the receiver. Although we could only measure a single polarization in each antenna at a given time, we sampled all four polarized correlations (LL, LR, RL, and RR) on each baseline by switching antennas between LCP and RCP in period 16 Walsh function patterns (e.g., Rao 1999). For 20 s integrations, a full cycle required just under 7 minutes. These observations were made during the commissioning phase of the SMA polarimetry hardware; details of this instrument can be found in D. P. Marrone (2006, in preparation).

TABLE 1
OBSERVING PARAMETERS

Date	τ_{337}[a]	$N_{\rm ant}$	$t_{\rm int}$ (minutes)
2004 May 25	0.16	7	100
2004 May 26	0.28	6	160
2004 Jul 5	0.11	7	160
2004 Jul 6	0.15	7	180
2004 Jul 7	0.29	6	170
2004 Jul 14	0.23	6	100

[a] Mean zenith opacity at the local oscillator frequency of 337 GHz.

The conversion of LP to CP was not perfect, but we calibrated the (frequency dependent) leakage of cross-handed polarization into each CP state of each antenna in order to properly determine source polarizations. We used a long observation of a polarized point source (in this case, the quasar 3C 279) to simultaneously solve for the quasar polarization and leakage terms (e.g., Sault et al. 1996). This polarization calibration was performed twice, on May 25 and July 14, yielding consistent leakages. The derived polarization leakages were at or below 3% in the USB and 5% in the LSB, with the exception of antenna 3, which used a sapphire wave plate with different frequency response and poorer performance (6% LSB leakage) than the other wave plates. Theoretical considerations of our design suggest that the real components of the L→R and R→L leakages should be identical for a given wave plate at a given frequency, and a comparison of the results on the two nights (a total of four measurements of each real component) show that the rms variations in the measured leakage terms were below 1% for all antennas except antenna 7. One measured leakage on July 14 was responsible for this antenna's large rms, and because of the disagreement between the real part of the L→R and R→L leakages, we know that this measurement was in error. Using the same comparison on the other antennas, we found that on average the solutions for this date were of poorer quality, probably due to the difference in weather. Accordingly, we adopted the May 25 leakage values for all dates, although that required that we not use antenna 8, which was absent from that calibration track. Errors in the leakage calibration produce effects of varying importance, as outlined in Sault et al. (1996); the most important for our purposes are the contamination of Q and U by Stokes I due to errors in the determination of the leakage calibrator polarization. We have examined this effect by comparing the Q and U fractions across sidebands on the high signal-to-noise ratio 3C 279 data sets of May 25 and July 14; the two sidebands should give identical measurements of Q and U from the source, and differences can be ascribed to noise in the images and the difference of the independent errors in the leakage solutions in the two sidebands. With this procedure we found no inter-sideband differences that were consistent across the two data sets, and the

[2] The Submillimeter Array is a joint project between the Smithsonian Astrophysical Observatory and the Academia Sinica Institute of Astronomy and Astrophysics and is funded by the Smithsonian Institution and the Academia Sinica.

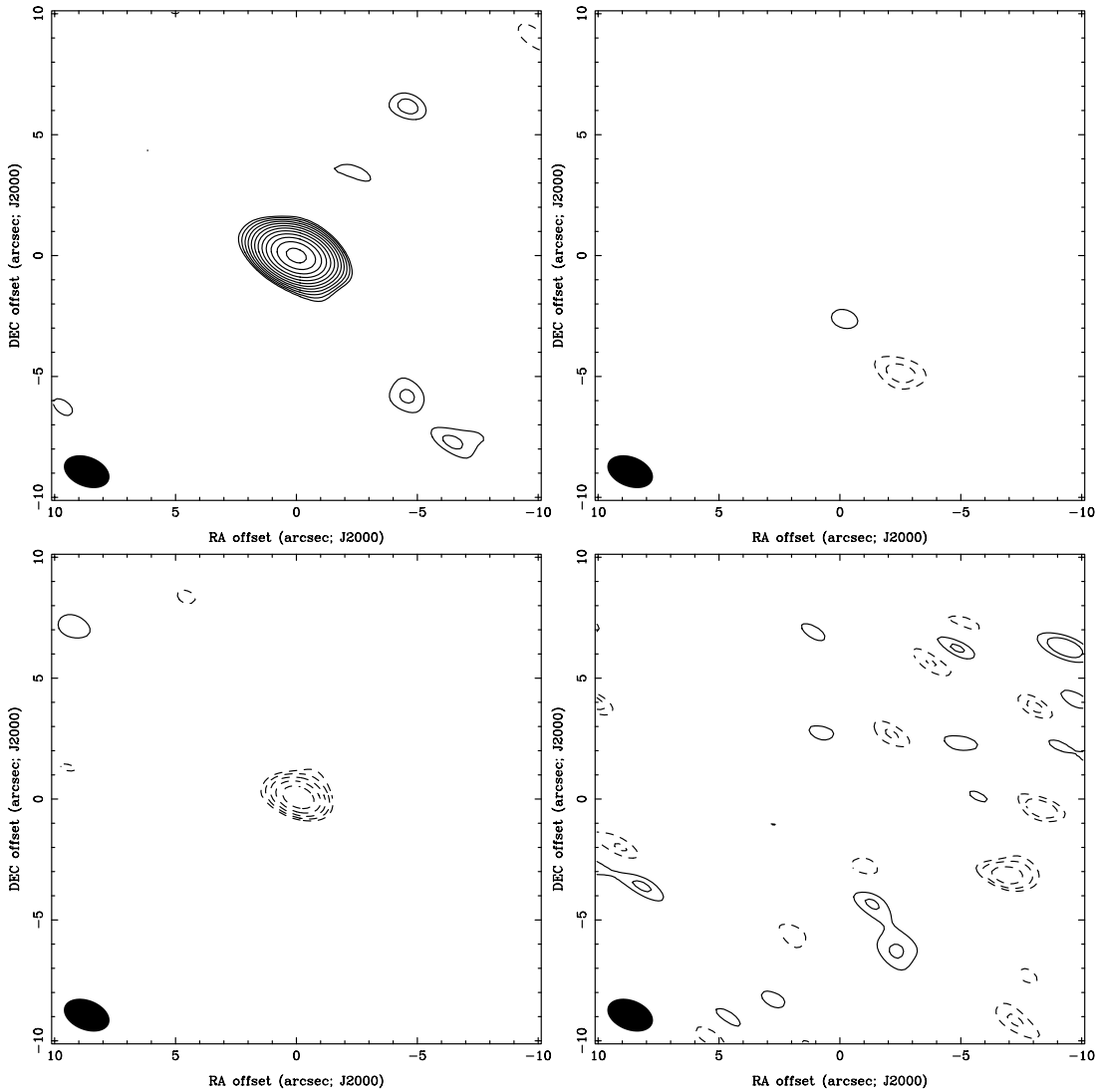

FIG. 1.—Sample Stokes images of Sgr A*, from the USB data (341.7 GHz) of 2004 May 25. The synthesized beam is $2''.0 \times 1''.2$. Panels clockwise from top left show *I*, *Q*, *V*, and *U*. Contours are spaced by geometrical factors of $\sqrt{2}$. For Stokes *I*, they are drawn at −4.2 (absent), −3, 3, 4.2, 6, 8.5, 12, 17, 24, 34, 48, 68, 96, and 136 times the 25 mJy beam^{-1} noise in the image, and for *Q*, *U*, and *V*, they are drawn at −12, −8.5, −6, −4.2, −3, 3, 4.2, and 6 (absent in all three images) times the 15 mJy beam^{-1} rms noise in the *Q* and *U* images (0.4% of $I_{\rm peak}$). The *V* contours match the *Q* and *U* contours to highlight the increased noise introduced by the contamination of *V* by *I*, which is due to relative gain variations between LCP and RCP.

differences present were consistent with the noise level, roughly 0.3% or smaller. Because an important part of our analysis is the comparison of position angles across sidebands, we had to ensure that the calibration did not create a position angle offset between the sidebands. Fortunately, although leakage errors could introduce spurious Stokes *Q* or *U* polarization, the phase difference between the RCP and LCP feeds, corresponding to a rotation of the sky polarization, is identically zero, because each pair of CP feeds is in reality a single LP feed looking through both crystal axes of the same wave plate. Therefore, the only way to create a relative position angle difference between the sidebands would be through the leakage errors and the resulting contamination of *Q* and *U*, an effect that appears to be small in our data.

The flux density scale was derived from observations of Neptune on all nights except May 25 and July 14. We expect that the absolute calibration will be accurate to about 25% on these nights. The May 25 flux density scale was transferred from three quasars that were also observed on May 26; these appeared to have the same relative flux densities on both nights to better than 10%, consistent with the overall uncertainty on that night, so we do not expect that the May 25 flux densities are any more uncertain than the others. The July 14 data were obtained in an engineering track primarily aimed at obtaining a second polarization calibration, so only three sources are present (Sgr A*, 3C 279, and 1743−038). Fortunately, 1743−038 has been very stable during more than two years of monitoring observations with the SMA (an rms flux density variation of only 20% in that time; M. Gurwell 2005, private communication), with even smaller (<10%) variations observed from July 5 to July 7, so we have used it as our flux density standard for the final track.

The data were averaged over the 7 minute polarization cycle to simulate simultaneous measurement of all four polarized visibilities and were then phase self-calibrated using the LL and RR visibilities. Quasars were interleaved into the observations of Sgr A* to allow variability monitoring and independent gain calibration. Transferring gains from the quasars, rather than self-calibrating, generally resulted in slightly lower signal-to-noise ratios but did not change the polarization. We attribute the increased noise (∼20%) to the 16°–40° angular separation between Sgr A* and the quasars. Following calibration, each sideband was

TABLE 2
340 GHz Polarization Measurements of Sagittarius A*

Date	I (Jy)	Q (mJy)	U (mJy)	V (mJy)	m (%)	χ (deg)
2004 May 25:						
USB	3.79 ± 0.03	9 ± 15	−244 ± 15	−5 ± 22	6.43 ± 0.39	136.1 ± 1.7
LSB	3.79 ± 0.02	13 ± 17	−201 ± 17	−9 ± 21	5.28 ± 0.45	136.8 ± 2.4
Both	3.79 ± 0.02	13 ± 11	−230 ± 11	−5 ± 17	6.07 ± 0.28	136.7 ± 1.3
2004 May 26:						
USB	3.19 ± 0.03	145 ± 20	−97 ± 20	−14 ± 21	5.43 ± 0.63	163.0 ± 3.3
LSB	3.11 ± 0.02	104 ± 18	−138 ± 18	−10 ± 22	5.53 ± 0.58	153.5 ± 3.0
Both	3.16 ± 0.02	118 ± 13	−138 ± 13	−17 ± 19	5.75 ± 0.43	155.3 ± 2.1
2004 Jul 5:						
USB	3.23 ± 0.04	42 ± 14	−267 ± 14	−37 ± 17	8.35 ± 0.44	139.5 ± 1.5
LSB	3.13 ± 0.02	41 ± 12	−273 ± 12	−19 ± 17	8.84 ± 0.38	139.3 ± 1.2
Both	3.20 ± 0.02	42 ± 10	−270 ± 10	−38 ± 13	8.52 ± 0.31	139.5 ± 1.0
2004 Jul 6:						
USB	3.19 ± 0.02	58 ± 21	−169 ± 21	−15 ± 25	5.56 ± 0.65	144.4 ± 3.3
LSB	3.15 ± 0.03	29 ± 18	−164 ± 18	−16 ± 22	5.27 ± 0.56	140.1 ± 3.0
Both	3.18 ± 0.02	52 ± 15	−177 ± 15	−18 ± 19	5.78 ± 0.49	143.2 ± 2.4
2004 Jul 7:						
USB	2.71 ± 0.03	38 ± 22	−35 ± 22	−8 ± 29	1.72 ± 0.82	158.8 ± 13.7
LSB	2.78 ± 0.04	31 ± 22	−67 ± 22	−13 ± 38	2.53 ± 0.80	147.6 ± 9.0
Both	2.75 ± 0.03	44 ± 17	−49 ± 17	−17 ± 25	2.32 ± 0.61	156.1 ± 7.5
2004 Jul 14:						
USB	3.00 ± 0.03	37 ± 27	−243 ± 27	14 ± 32	8.14 ± 0.91	139.3 ± 3.2
LSB	3.00 ± 0.03	29 ± 19	−175 ± 19	−17 ± 25	5.87 ± 0.64	139.7 ± 3.1
Both	3.02 ± 0.03	75 ± 16	−236 ± 16	−15 ± 24	8.17 ± 0.55	143.8 ± 1.9
All days:						
USB	3.33 ± 0.02	57 ± 10	−197 ± 10	−9 ± 15	6.15 ± 0.29	143.1 ± 1.3
LSB	3.29 ± 0.02	49 ± 10	−202 ± 10	−8 ± 13	6.32 ± 0.29	141.8 ± 1.3
Both	3.31 ± 0.02	59 ± 7	−204 ± 7	−17 ± 11	6.39 ± 0.23	143.1 ± 1.0

Note.—Errors in the flux density columns are from the image rms only; they do not include the 25% absolute calibration uncertainty, which applies equally to all flux densities and does not affect the m or χ columns.

separately imaged in Stokes I, Q, U, and V, using only baselines longer than 20 kλ, and then cleaned. Sample Stokes images are shown in Figure 1. On July 14, due to poorer coverage in the uv-plane in the short track, we increased the cut to 30 kλ. Flux densities were extracted from the center pixel of each image, and these are listed in Table 2. We also examined the polarization by fitting point sources to the central parts of the images; the point-source flux densities matched well with those obtained from the central pixel when the signal was well above the noise, but the point-source positions and peak flux densities became erratic for low signal-to-noise ratio images (most Stokes Q and V images). Table 2 also includes the polarization fraction (m), which has been corrected for the noise bias (through quadrature subtraction of a 1 σ noise contribution; e.g., Wardle & Kronberg 1974), and the electric vector position angle [χ, determined as $2\chi = \tan^{-1}(U/Q)$].

3. RESULTS

3.1. *Linear Polarization*

The polarization fraction and position angle for each sideband on each night are plotted in Figure 2. It can be seen from the figure and the data in Table 2 that we have clear detections of the linear polarization in both sidebands on all nights. Among the six nights of our observations, July 7 stands out for its low polarization fraction, around 2%. The polarization was only detected at the 2–3 σ level in each sideband, so the polarization position angle was poorly constrained. This is the lowest linear polarization fraction measured at or above 150 GHz, the lowest frequency at which polarization has been detected. The weather on this night was the poorest of all the tracks, but only marginally worse than May 26, which did not show an unusually low polarization. Other sources in the July 7 track with measurable polarization, such as 3C 279, did not show a significantly lower polarization than on other nights, as one might have expected from a systematic problem in that track. An obvious systematic error would be a substantial change in the leakages with respect to previous nights; this would most easily be caused

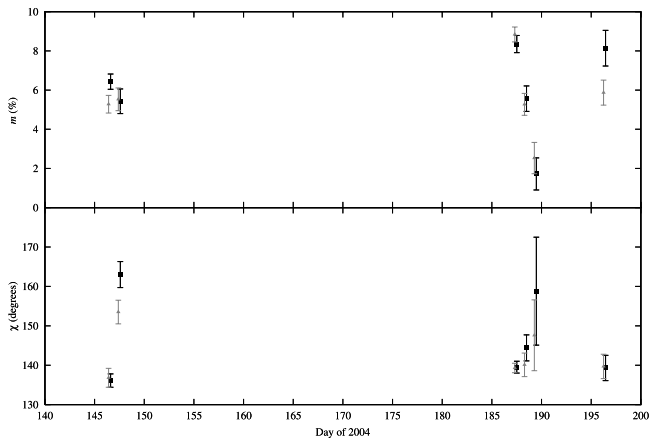

Fig. 2.—Plots of the 340 GHz Sgr A* polarization fraction (m; *top*) and position angle (χ; *bottom*). The USB (*black squares*) and LSB (*gray triangles*) data are plotted separately for each night. The two sidebands are slightly offset in time for clarity, but both sample the same time interval. The large χ error bars on day 189 (July 7) are due to the low polarization signal on that night.

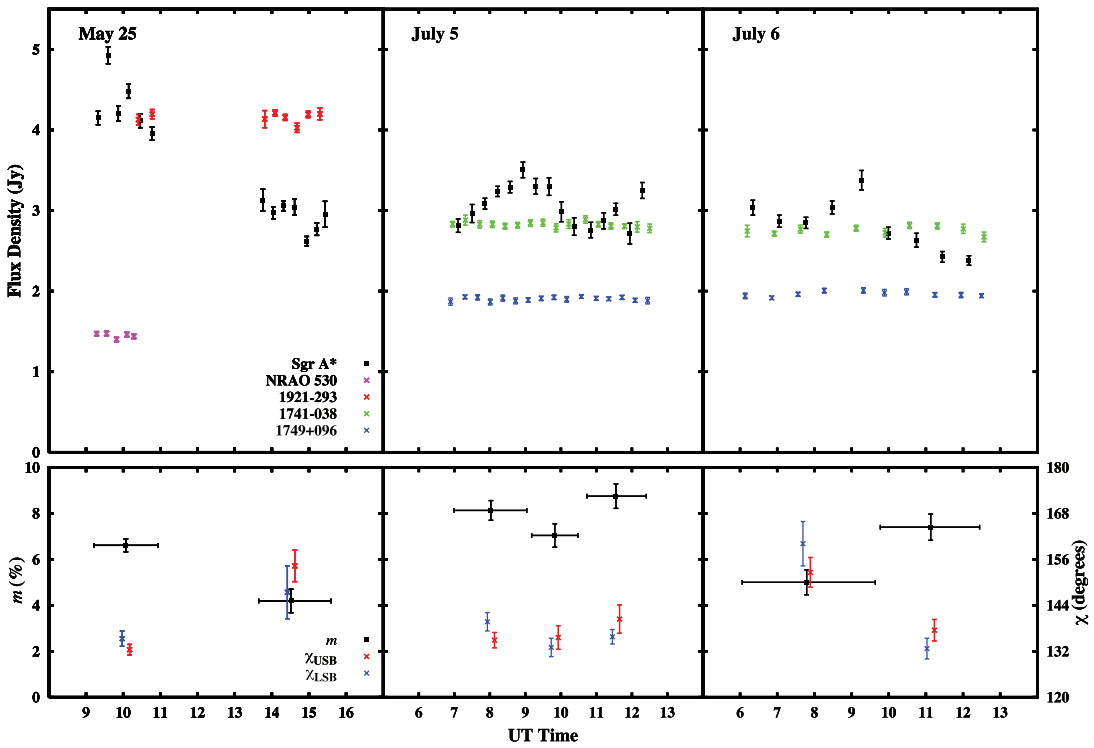

FIG. 3.—Variability in the total intensity (*top*) and polarization (fraction and position angle; *bottom*) of Sgr A* at 340 GHz. The three nights with the best weather are shown, as these permit the most accurate determinations of the polarization variation. The total intensity light curves of the quasar calibrators, 1741−038, 1749+096, and 1921−293, are also shown. In the lower plots, the binned intervals are demarcated by the horizontal bars on the polarization fraction points. This polarization fraction is the double-sideband value. The USB and LSB position angles sample the same time bin but have been offset slightly from the bin center for clarity.

by large changes to the alignment of the polarization hardware. However, the hardware was not moved between installation on July 5 and removal after the July 7 track, and the July 5 and 6 tracks show substantially larger polarization, so this possibility seems very unlikely. Moreover, because the leakages measured on July 14 are consistent with the May 25 leakages, as discussed in § 2, any change between July 6 and 7 would have to have been reversed when the hardware was reinstalled on July 14. This low polarization fraction, along with the unusually high polarization two nights before, clearly demonstrates that the polarization fraction is variable. Moreover, the polarization variations are present both in the polarization fraction and the polarized flux density, even after accounting for the 25% uncertainty in the overall flux density scale, and are not merely the result of a constant polarized emission component with a changing total intensity.

Variability was also observed in the polarization position angle. Polarization over four of the nights ranged between roughly 137° and 143°, at a weighted average position angle of 139°.6. The position angle determined for May 26 differed significantly from this range, and July 7 had an extremely uncertain position angle due to the very low polarization fraction. Neither the combined six-night data set nor the individual nights showed significant inter-sideband differences, with the possible exception of May 26. On that night $\chi_{\rm LSB} - \chi_{\rm USB} = (153^\circ.5 \pm 3^\circ.0) - (163^\circ.0 \pm 3^\circ.3) = -9^\circ.5 \pm 4^\circ.5$, which is marginally significant for the quoted errors. As we discussed in § 2, although it is possible for Stokes I to contaminate Q and U (which determine χ), this appears to be unimportant in these data. The 0.3% limit on this effect is smaller than the Q and U errors on May 26, which are 0.6% of the Stokes I. Furthermore, any other systematic source of inter-sideband position angle offsets would show up equally on all nights, but the six-night average $\chi_{\rm LSB} - \chi_{\rm USB}$ is $1^\circ.3 \pm 1^\circ.8$, which is consistent with zero. The May 26 result is considered further in the context of a Faraday rotation measure in § 4.1.

3.2. *Circular Polarization*

Neither the averaged data nor the individual nights show CP at a level that is significant. The greatest deviation from zero is -38 ± 13 mJy on July 5, corresponding to $-1.2\% \pm 0.4\%$. However, in addition to the quoted error, which is the measured noise in the cleaned map, there are well-known systematic effects. The MIRIAD reduction package (Sault et al. 1995) uses linearized equations when solving for the polarized leakages, ignoring second-order terms in the leakages (d) and linear polarization fraction. These terms contribute a systematic error in Stokes V of the form Id^2 and md (Roberts et al. 1994), which may be on the order of a few tenths of a percent for our leakages and the polarization of Sgr A*. Moreover, the small difference in the sample times of the LL and RR correlations on a given baseline permit gain differences due to weather, pointing, and system changes to introduce differences between the LL and RR visibilities that would not be present if these were actually measured simultaneously (as our reduction assumes). These gain variations contaminate Stokes V with Stokes I and make the value of V at the peak of the I map more uncertain than the map rms would indicate. The average of all six tracks shows $-0.5\% \pm 0.3\%$ CP, consistent with zero, with an additional systematic error of perhaps another 0.3%. The 0.5% sum of these errors can be taken as a limit on any persistent level of CP across the six nights and is the most stringent limit yet on CP in Sgr A* above 90 GHz.

3.3. *Intraday Variability*

Intraday variability in the total intensity (Stokes I), the polarization fraction, and position angle are shown in Figure 3.

The July 5–7 observations were obtained as part of a coordinated multiwavelength Sgr A* monitoring program, and the observed temporal variability in Stokes *I* on these nights is discussed in conjunction with results at other wavelengths in Eckart et al. (2006). In order to prevent antennas with variable performance from falsely modulating Stokes *I*, we use only the five antennas with the best gain stability for these light curves. Slow variations in the gain of the other antennas are likely due to pointing errors. We have reduced the effects of changing spatial sampling of extended emission by removing the two baselines that project to less than 24 kλ (angular scales >9″) during the Sgr A* observations. Further details of the light curve reduction can be found in Eckart et al. (2006). The variability in the linear polarization is much harder to measure; with signals 1–2 orders of magnitude weaker than Stokes *I*, it is difficult to obtain reliable results from a subdivided track, and we could not be as selective about which data to exclude in the hope of removing the imprint of instrumental variations from the polarization variation. Accordingly, polarized light curves could not be reliably extracted for May 26 and July 14 due to poor weather, nor for July 7, due to both weather and very low polarization fraction. The remaining three nights have been subdivided into two or three segments at boundaries in the Stokes *I* curves, and the polarization has been extracted as described in § 2. The large (160 minute) gap on May 25, due to instrument difficulties, served as one of the boundaries.

A great deal of variability is visible in the Stokes *I* curve on all three nights, with the most notable feature being the ~1.5 Jy difference between the flux densities of the first and second halves of the May 25 data. No such difference shows up in the light curve of the calibrator, 1921−293, a source at nearly identical declination, suggesting that this result is not an instrumental artifact. Clear polarization variability is also measured on May 25 and July 6 in both *m* and χ. At all times the position angles in the USB and LSB are found to be very similar, as was observed in the full track averages reported above.

4. DISCUSSION

4.1. *Rotation Measure*

The rotation measure associated with a plasma screen located between the source and observer can be inferred from the measurement of χ at two frequencies, since it introduces a frequency-dependent change in the position angle given by

$$\chi(\nu) = \chi_0 + \frac{c^2}{\nu^2}\mathrm{RM}, \tag{1}$$

where the RM is given by (e.g., Gardner & Whiteoak 1966)

$$\mathrm{RM} = \left(8.1 \times 10^5\right) \int n_e \boldsymbol{B} \cdot d\boldsymbol{l} \tag{2}$$

for the electron density n_e in units of cm^{-3}, the path length $d\boldsymbol{l}$ in units of pc, and the magnetic field $\boldsymbol{B}$ in units of Gauss. The greatest obstacle to such a detection, as previously noted, is the variability in the polarization, which may prevent polarization measured at different times from being reliably compared.

The best method for measuring the RM from our data comes from the observed difference in the simultaneous position angles in the USB and LSB. If we apply equation (1) to the two sideband frequencies of these observations, for position angles in units of degrees, we obtain

$$\mathrm{RM} = (3.7 \times 10^5)(\chi_{\mathrm{LSB}} - \chi_{\mathrm{USB}}). \tag{3}$$

Equation (3) implicitly assumes that the Faraday rotation occurs outside of the plasma responsible for the polarized emission. This assumption seems reasonable for Sgr A*; very long baseline interferometry (VLBI) measurements (Krichbaum et al. 1998; Shen et al. 2005; Bower et al. 2004) suggest intrinsic sizes of 13–24r_{S} at 215, 86, and 43 GHz, and for reasons described in § 4.2 we expect little contribution to the RM inside 300r_{S}. One other potential complication arises if the source polarization changes with radius and the two frequencies being compared probe different radii. For our 3% sideband separation, and if we assume that the polarized submillimeter emission is thermal synchrotron (as is expected in ADAF models; Yuan et al. 2003), we expect a 5% opacity difference between our sidebands, while for nonthermal synchrotron emission (taking an electron energy spectral index of 2–3.5; e.g., Markoff et al. 2001; Yuan et al. 2003) the difference is 9%–12%. Emission will be contributed from a range of radii around the $\tau = 1$ surfaces, so we would have to postulate a large gradient in the source polarization to produce a large intrinsic inter-sideband polarization difference over such a small frequency range. Finally, the 2 GHz bandwidth at 340 GHz limits the allowed RM to approximately 2×10^7 rad m^{-2} if polarization is detected, as this RM would rotate the polarization by more than a radian across the band and wash out the signal (bandwidth depolarization). For highly polarized emission, the vector average of the polarization may still be detectable, but the position angles of the two sidebands are very unlikely to agree in this case. We can therefore ignore the possibility of full 180° wraps between sidebands, as a wrap requires a RM of 7×10^7 rad m^{-2}.

As is clear from Table 2, we do not see a significant change in the position angle between the two SMA sidebands on most of the observing nights (disregarding the uncertain position angle of July 7). In the most sensitive track, July 5, the sideband difference places a 1 σ limit of 7.1×10^5 rad m^{-2} on the RM on that particular night, which is the most sensitive limit to date from simultaneous interferometric observations. If the full data set is considered together (i.e., with Stokes images derived from the ensemble of data), the limit drops by a small amount to 6.8×10^5 rad m^{-2}, although if the RM is varying between observations this average will not actually represent a measurement of a RM. It should be noted here that the broadband observations of Aitken et al. (2000) were able to place a similar limit of approximately 5×10^5 rad m^{-2} on the RM in 1999 August because of the large bandwidth of their 150 GHz bolometer.

The May 26 sideband difference of $-9\overset{\circ}{.}5 \pm 4\overset{\circ}{.}5$ is possibly significant, with an inferred rotation measure of $(-3.5 \pm 1.7) \times 10^6$ rad m^{-2}. If this RM had been present on the previous night, it would have shown up as a similarly large sideband difference instead of the observed $0\overset{\circ}{.}7 \pm 3\overset{\circ}{.}1$, which corresponds to a RM of $(0.3 \pm 1.1) \times 10^6$ rad m^{-2}. We can check the large RM by comparing the position angles on May 25 and 26, on the assumption that the emitted polarization (χ_0 from eq. [1]) is constant over timescales of a few days and observed position angle changes are due to RM changes. At this frequency, the relationship between the position angle change ($\Delta\chi$, in units of degrees) and the RM change is (see eq. [1])

$$\Delta\mathrm{RM} = (2.2 \times 10^4)\Delta\chi. \tag{4}$$

We observed an increase in the position angle from May 25 to May 26 of $18\overset{\circ}{.}6 \pm 2\overset{\circ}{.}5$. If this is not a change in the intrinsic polarization, it corresponds to an increase in the RM of 4×10^5 rad m^{-2}, which is inconsistent with the small sideband difference on May 25 and the large difference on May 26. The position

angle is 180° degenerate, however, and a change in χ of $18\overset{\circ}{.}6 - 180^\circ = -161\overset{\circ}{.}4$ requires a RM change of -3.6×10^6 rad m^{-2}, which agrees well with the RM inferred from the May 26 sideband difference. It is therefore possible that we have observed a large change in the RM between these two nights, with the May 26 value far in excess of the limits on the other five nights. We discuss this further in § 4.2.

In the existing polarization data at 230 and 340 GHz, the position angle seems to frequently return to the same value. The Bower et al. (2005) 230 GHz data are clustered around 111° between 2002 October and 2004 January, while four of our observations at 340 GHz have a mean position angle of 140°. Assuming that these two angles sample the same χ_0 (no source polarization changes between the two observing periods or observing frequencies), we can infer a "quiescent" RM of -5.1×10^5 rad m^{-2}. This is just below the RM upper limit from our most sensitive night. If the idea of a quiescent RM is correct, then the change in the mean 230 GHz position angle observed between early 2002 (Bower et al. 2003) and 2003 (Bower et al. 2005) merely reflects a change in this RM by -3×10^5 rad m^{-2}. This implies that the quiescent RM in early 2002 was around -8×10^5 rad m^{-2}, which is conveniently below the detection limit of the Bower et al. (2003) observations. If this scenario is correct, the RM should be detectable by the SMA at 230 GHz, where it would be observable as a 5° sideband difference.

4.2. *Accretion Rate Constraints*

Much of the importance placed on the RM determination stems from its use as a probe of the accretion rate near the black hole. However, the interpretation of a RM detection, or limit, in terms of an accretion rate requires a model for the density and magnetic field in the accretion flow, as these quantities actually determine the RM through equation (2).

To estimate the RM predicted for a variety of accretion models, we make several simplifying assumptions. First, we assume a generic picture with a central emission source surrounded by a roughly spherical accretion flow. Given the previously mentioned limits on the millimeter size of Sgr A*, we could also accommodate models where the observed 340 GHz emission arises in a small jet component, as the jet would have to lie within $\sim 10 r_S$ of the black hole and would effectively be a central emission source as seen from a Faraday screen tens to hundreds of r_S further out. We characterize the radial density profile, $n(r)$, as a power law,

$$n(r) = n_0 (r/r_S)^{-\beta}, \tag{5}$$

where $r_S = 2GM_{BH}/c^2$ is the Schwarzschild radius of Sgr A* (10^{12} cm for $M_{BH} = 3.5 \times 10^6\ M_\odot$), and n_0 is the density at this radius. In the case of free-falling gas we have $\dot{M}(r) \propto r^p$ with $\beta = 3/2 - p$, as in Blandford & Begelman (1999). For spherical accretion (Bondi 1952) or an advection-dominated accretion flow (ADAF; Narayan & Yi 1994), we have $\beta = 3/2$, while for a convection-dominated accretion flow (CDAF; Quataert & Gruzinov 2000a), formally an $\dot{M} = 0$ limiting case of convection-frustrated accretion, we have $\beta = 1/2$. Intermediate values are also possible: the best-fit radiatively inefficient accretion model in Yuan et al. (2003) has $\beta = 0.8$, and accretion flow simulations (e.g., Pen et al. 2003) typically produce values between 1/2 and 1 (Quataert 2003). We take the ADAF and CDAF values as bounds on β (i.e., from 1/2 to 3/2).

Rather than using a separate parameter to describe the magnetic field profile, we tie it to the density by assuming equipartition between magnetic, kinetic, and gravitational energy, as many other modelers have done (e.g., Melia 1992). For pure hydrogen gas, with the use of equation (5), we obtain

$$B(r) = \sqrt{4\pi c^2 m_H n_0} \left(\frac{r}{r_S}\right)^{-(\beta+1)/2}. \tag{6}$$

We additionally assume that the magnetic field contains no reversals along the line of sight and is entirely radial, which should contribute only a small error unless the field is very nearly toroidal. The former simplification is a good approximation for strongly peaked RM versus r profiles (large β), where only a small radial range contributes significantly. For smaller values of β and many field reversals, the effective field will only drop as the square root of the number of reversals.

In the Sgr A* accretion flow we expect that the electron temperature (T_e) will rise to smaller radii, eventually bringing the electrons to relativistic temperatures ($T_e > 6 \times 10^9\ \mathrm{K} = m_e c^2/k$) at some radius r_{in}. The RM contribution from relativistic electrons is suppressed [by as much as $\log(\gamma)/2\gamma^2$ for the Lorentz factor γ in the ultrarelativistic thermal plasma limit; Quataert & Gruzinov 2000b], so we approximate this effect by truncating the RM integration at r_{in} and by treating r_{in} as a variable. From the density profile, if we assume that gas at r_{in} is in free fall, we can determine a mass flux across the $r = r_{in}$ surface:

$$\begin{aligned}\dot{M}_{in} &= 4\pi r_{in}^2 m_H n(r_{in}) v(r_{in}) \\ &= 4\pi r_S^2 m_H n_0 c (r_{in}/r_S)^{3/2-\beta}.\end{aligned} \tag{7}$$

This equation does not require that the density profile be followed down to $r = r_S$; $n_0 = n(r_S)$ is merely a convenient quantity to normalize the power-law density relation we are assuming for larger radii. The mass flux at r_{in} ($\dot{M}_{in}$) can be taken to be an upper limit on the accretion rate at r_S, but the true rate of accretion onto the black hole could be lower if the loosely bound plasma falling from r_{in} escapes as a wind or jet. By substituting equations (5), (6), and (7) into equation (2) and converting $\dot{M}_{in}$ to units of $M_\odot$ yr^{-1} and r to r_S, we obtain

$$\begin{aligned}\mathrm{RM} = &\left(3.4 \times 10^{19}\right) \left(\frac{M_{BH}}{3.5 \times 10^6\ M_\odot}\right)^{-2} \\ &\times r_{in}^{(6\beta-9)/4} \dot{M}_{in}^{3/2} \int_{r_{in}}^{r_{out}} r^{-(3\beta+1)/2}\, dr.\end{aligned} \tag{8}$$

Integrating and simplifying yields

$$\begin{aligned}\mathrm{RM} = &\left(3.4 \times 10^{19}\right) \left[1 - (r_{out}/r_{in})^{-(3\beta-1)/2}\right] \\ &\times \left(\frac{M_{BH}}{3.5 \times 10^6\ M_\odot}\right)^{-2} \left(\frac{2}{3\beta - 1}\right) r_{in}^{7/4} \dot{M}_{in}^{3/2}.\end{aligned} \tag{9}$$

To obtain an RM from a given β and $\dot{M}_{in}$, we must also choose r_{in} and r_{out}. The inner radius will vary by model, but it is typically around $300 r_S$ (e.g., Yuan et al. 2003). For these calculations we consider values of r_{in} from $300 r_S$ to $3 r_S$ in order to account for variations among models and to allow for the possibility that the electrons do not become highly relativistic interior to r_{in}, in which case the RM would not be strongly suppressed. The outer radius depends on the coherence of the radial field. We examine two cases: a fully coherent field ($r_{out} \approx \infty$), and a field that persists for a factor of 3 in radius from r_{in}.

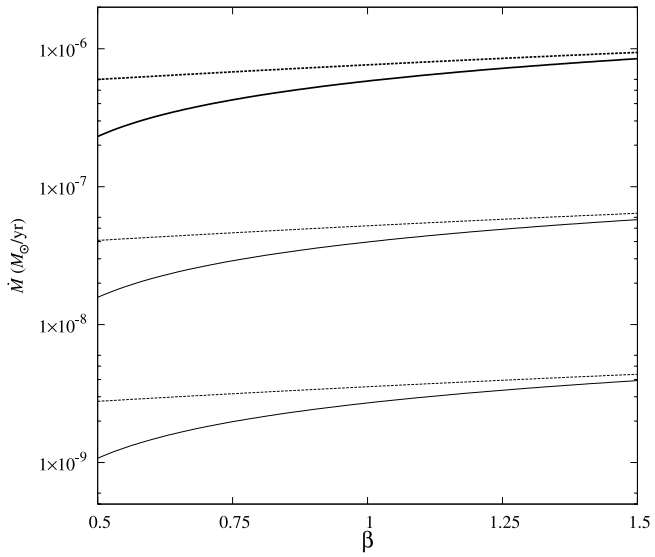

FIG. 4.—Accretion rate limits imposed by the rotation measure limit of 7×10^5 rad m^{-2} as a function of the density power law, given the accretion model described in § 4.2. The accretion rate plotted here is measured at the radius where the electrons become relativistic, $r_{\rm in}$; extrapolation to the black hole event horizon is discussed in § 4.2. Two sets of curves are plotted (see eq. [9]): three for a magnetic field that is coherent to large radius (*solid lines*), and three for a field that is coherent over a smaller range ($r_{\rm out}/r_{\rm in} = 3$; *dashed lines*). Within each set, the lines from thickest to thinnest represent $r_{\rm in} = 300r_{\rm S}$, then $30r_{\rm S}$, and finally $3r_{\rm S}$.

Figure 4 shows the accretion rate limits imposed by our RM limit of 7×10^5 rad m^{-2}, based on the model described above. From the two choices of $r_{\rm out}$ we see that the effect of the magnetic field coherence is larger at small values of β. As mentioned before, for steep density profiles (large values of β) we expect that only a small range in radius around $r_{\rm in}$ contributes to the RM, making the inferred accretion rate limit insensitive to the field coherence length. If we assume that the density profile follows equation (5) down to $r = r_{\rm S}$, our model imposes accretion rate limits that are a factor of $\dot{M}(r_{\rm S})/\dot{M}_{\rm in} = (r_{\rm in}/r_{\rm S})^{\beta-3/2}$ lower than those in Figure 4, but the transition to supersonic flow makes this density extrapolation uncertain. However, in cases like the basic ADAF model (Narayan & Yi 1995) in which the electron temperature ceases to rise at small radii and the electrons are only marginally relativistic, integration to smaller radii (the lower sets of curves) may set more relevant (and lower) accretion rate limits. In fact, by taking $\beta = 3/2$ and $r_{\rm in} = 30r_{\rm S}$, we roughly have the ADAF Bondi model used in Quataert & Gruzinov (2000b), and we reproduce their $\dot{M}$ limit of $10^{-7}\ M_\odot$ yr^{-1}. The high- and low-β limits are similar, but the field coherence is a larger concern for shallow profiles. Since the prototype for a low-β model is a highly convective flow, we can expect a tangled field, but in this case the accretion rate limit (proportional to $B^{-2/3}$) will increase only as $\dot{M} \propto N^{1/3}$ for N field reversals. In summary, the figure shows that for any choice of density profile, the maximum allowed accretion rate is $10^{-6}\ M_\odot$ yr^{-1} and may be much lower. This is an order of magnitude below the gas capture rate of $10^{-5}\ M_\odot$ yr^{-1} inferred from X-ray observations (Baganoff et al. 2003; Yuan et al. 2003) and from simulations of stellar winds in the Galactic center (e.g., Quataert 2004; Cuadra et al. 2006). It is therefore likely that there is substantial mass lost between the gas capture at $r \sim 10^5 r_{\rm S}$ and the event horizon.

Finally, this model of the accretion flow can be used to examine the proposed -3.5×10^6 rad m^{-2} RM from May 26 (§ 4.1). This RM would require a change of more than 2×10^6 rad m^{-2} between consecutive nights. This is very large compared to the RM changes implied by other position angle changes (again, assuming that the source polarization remains constant). On the basis of the four other nights with strong polarization detections, all of which have position angles near 140°, the peak-to-peak change in χ corresponds to an RM change of 1.5×10^5 rad m^{-2}, and the rms variation is only 5×10^4 rad m^{-2}. The largest change on similar timescales (days to weeks) observed at 230 GHz is 3×10^5 rad m^{-2} (between 2003 December 27 and 2004 January 5; Bower et al. 2005). The longer timescale 230 GHz position angle changes and the difference between our position angles and the Aitken et al. (2000) 350 GHz position angle (reinterpreted as described in § 4.3 or otherwise) also correspond to RM changes of a few times 10^5 rad m^{-2}. We expect that these variations are not more than order unity fractional RM changes, so they are all quite consistent with our inferred -5×10^5 rad m^{-2} quiescent RM from § 4.1. The May 26 RM would then correspond to a factor of 7 increase in the density or line-of-sight magnetic field. Such a change is difficult to accomplish with any density profile but is particularly difficult for small values of β, where the entire line of sight contributes significantly to the RM. If the fluctuation is real, it suggests a steep density profile, as the associated density/field change should not be extended over decades of radius. Unless such an event is observed again in future observations, the more likely interpretations appear to be that the position angle change from May 25 represents a RM fluctuation of 4×10^5 rad m^{-2} observed between consecutive nights or a transient change in the source polarization, and the May 26 difference in the USB and LSB position angles is merely a 2 σ measurement noise event.

4.3. *Linear Polarization and Variability*

Our 340 GHz observations show a typical polarization fraction of 6.4%, with a range of 2.3%–8.5%, and an rms variation of 2.0%. This is comparable to the ~7.5% mean, 4.6%–13.6% range, and 2.2% rms measured at 230 GHz by Bower et al. (2003, 2005). The range of observed polarization is lower at 340 GHz than it is at 230 GHz, and the mean is slightly lower as well. It is difficult to explain a lower observed polarization fraction (and comparable variability) at higher frequencies with beam depolarization models (Tribble 1991), as Faraday rotation and the resulting dispersion in polarization directions decreases with increasing frequency. If the polarization fraction decrease is intrinsic to the source and not generated in the propagation medium, it suggests that the magnetic field becomes increasingly disordered at smaller radii, as these observations should probe slightly smaller radii than the 230 GHz data. But across only 0.2 decades in frequency we expect little change in intrinsic polarization, so the difference, if present, may be best explained by time variability in the source polarization. To resolve this question, simultaneous or nearly coincident polarimetry at multiple frequencies with interferometer resolution is clearly desirable.

Bower et al. (2005) used the apparent stability of the 230 GHz polarization fraction to argue that the observed variations in the 230 GHz polarization position angle were more likely to be the result of changes in the rotation measure than due to intrinsic source changes. While our results do not refute this conclusion, they demonstrate that the polarization fraction is not stable, even over a single night. Note that two substantial excursions in the 230 GHz polarization fraction, one of which is labeled an "outlier" in Bower et al. (2005), probably represent real variations similar to those seen here but have lower significance because of the poorer sensitivity of their instrument.

The polarization fraction presented here is considerably lower than those measured in 1999 by Aitken et al. (2000): 13^{+10}_{-4}%

and 22^{+25}_{-9}% at 350 and 400 GHz, respectively. However, to determine the flux density of Sgr A*, Aitken et al. (2000) had to correct for the contamination from dust and free-free emission in their large primary beam (14″–12.″5 at the highest frequencies), and it is possible that they overcorrected for the dust emission, which would make the polarized component appear to be a larger fraction of the total flux density of Sgr A*. There is some support for this possibility from their measured flux densities: Sgr A* was found to be only 2.3 and 1 Jy at 350 and 400 GHz, while our data (see Table 2) and previous measurements between 300 and 400 GHz have found higher values of 2.6–3.8 Jy (Zylka et al. 1995; Serabyn et al. 1997; Pierce-Price et al. 2000). If we assume that their 350 GHz data are well calibrated (the 400 GHz calibration is more uncertain) and assume our 3.3 Jy flux density for Sgr A*, we can rederive the intrinsic polarization of Sgr A* using their Stokes Q and U decomposition method and find a polarization of 9% at 158°. The polarization fraction drops further as the assumed flux density for Sgr A* is increased, reaching 7.6% for 3.8 Jy. These values are within the polarization fraction variations we observe; one might expect that well-calibrated 400 GHz measurements could be interpreted similarly and that the polarization fraction need not rise steeply to high frequencies. In arriving at a flux density of 2.3 Jy for Sgr A*, Aitken et al. (2000) estimated the dust emission in their central pixel from the average of the surrounding pixels, so by increasing the contribution from Sgr A*, we are also suggesting that there is a deficit of dust emission in the central 14″ at 350 GHz. Unfortunately, our observations are poorly sampled at short spacings, but the available visibilities shortward of 20 kλ show little excess over the point-source flux density, consistent with such a central hole in the dust emission. The existence of this hole requires further confirmation, as could be achieved through simultaneous single-aperture and interferometer observations; our circumstantial evidence could be equally well explained if Sgr A* had a higher polarization fraction and lower flux density in 1999 (at the time of the Aitken et al. 2000 measurement) and if the emission in the central 30″ is distributed smoothly on scales smaller than 10″.

We observe variability on internight and intraday intervals in both the polarization and total intensity. The single-night flux densities that we measure fall within the range of previous observations, and the rms variation of 0.3 Jy, or 10%, matches the recent results of Mauerhan et al. (2005) at 100 GHz. Within nights, the Stokes I light curves in Figure 3 show unambiguous variations on timescales of hours, reminiscent of those seen at 100 and 140 GHz by Miyazaki et al. (2004) and Mauerhan et al. (2005). This is slower than the variations seen in the near-infrared and X-ray (e.g., Baganoff et al. 2001; Genzel et al. 2003), which seem to vary on hour timescales, with some features requiring only minutes. These slow changes suggest that opacity is obscuring our view of the very inner regions of the accretion flow, regions unobscured at NIR/X-ray wavelengths, even at 340 GHz. At slightly higher frequencies the inner flow may become visible, although many estimates of the optically thin transition frequency place it at or above 1 THz, a frequency that is difficult to access from the ground. It should be possible to search for the transition to optically thin emission using the change in the variability timescale; the more frequently proposed technique of looking for the turnover in the spectrum relies on precise flux density calibration at high frequencies, which is problematic because of contaminating emission in single-aperture beams and lack of unresolved calibrators in interferometers. A few instruments may be able to make these difficult observations before the Atacama Large Millimeter Array (ALMA): the SMA, or perhaps the Submillimeter Common-User Bolometer Array (SCUBA; Holland et al. 1999) on the JCMT at 650 GHz, and the Submillimeter High Angular Resolution Camera (SHARC II; Dowell et al. 2003) on the Caltech Submillimeter Observatory (CSO) at 650 or 850 GHz.

The intraday variations in the linear polarization shown in Figure 3 are the first linear polarization changes observed on intervals of hours rather than days. The three nights with time-resolved polarization measurements do not demonstrate a clear relationship between Stokes I and the polarization. For example, May 25 shows a very strong flare in I with m very close to our average values, followed in the second half of the track by a lower I and a below-average m. July 5 has the highest value of m of our six nights, along with 20% modulation in I, but the polarization fraction is not modulated significantly with the total intensity. Finally, on July 6 we see below-average m in a period of high I and above-average m with low I, the inverse of the relationship seen on May 25. That the polarization fraction may vary in multiple ways during flares in the total intensity could suggest that there are multiple mechanisms (of varying polarization) responsible for the submillimeter Stokes I variability, or that the I and m changes are not closely related. Diverse flare mechanisms could be expected to show different spectra at shorter wavelengths, so simultaneous infrared and X-ray data may be useful. However, on the basis of the infrequency of infrared and X-ray flares (Eckart et al. 2004) and the lack of coincident activity in these bands during the SMA observations on July 6 and 7 (Eckart et al. 2006), it seems that the small changes we observe in the submillimeter are often imperceptible at shorter wavelengths. Therefore, the best way to determine whether the polarization changes are internal or external may be to increase the time resolution in the polarization light curves. In these data we observe changes in m on the shortest interval we can measure, around 3 hr (on July 6). This is close to the variability timescale observed in the total intensity, which suggests that, given better time resolution, we may see that the changes in I and m have similar temporal characteristics and therefore arise from the same processes.

The m and χ curves seem to show more coordinated behavior than the total intensity and polarization do. Of the seven subnight intervals plotted in Figure 3, five show position angles close to the observed quiescent χ-value of 140°. Only in the two intervals with the lowest polarization, on May 25 and July 6, does χ deviate from this value, and if the deviations are caused by RM changes, then both would represent increases in the RM. None of the intervals provide evidence for a RM through inter-sideband differences in χ, but the largest change in χ between intervals, $-20.^{\circ}7 \pm 3.^{\circ}8$ on July 6, only requires a RM decrease of 5×10^5 rad m^{-2}, which is still below our detection limits. Here again we face the question of whether the source polarization or an external process is responsible for the variability we see. It is possible to explain the changes in χ with a two-component source, where the dominant polarization component is polarized close to the quiescent polarization direction and variable in amplitude, while the weaker component causes the polarization to deviate from 140° when the dominant component weakens. In this case we would expect to see a correlation between the polarization fraction and the position angle, something that is not excluded by our data. Such a source model is naturally identified with emission from a core and jet. A second model uses a turbulent plasma screen, in addition to the screen responsible for the putative mean RM (suggested by the difference in position angle between 230 and 340 GHz), to partially beam-depolarize the emission. The fact that χ seems to faithfully return to 140° implies that the source, or the source

plus a stable RM component, is separated from the changes that cause the depolarization and position angle change. With better time resolution and better sensitivity to RM, it should be possible to distinguish between these models.

5. CONCLUSIONS

Using the Submillimeter Array outfitted with polarization conversion hardware (D. P. Marrone 2006, in preparation), we have made sensitive measurements of the polarization of Sgr A* at 340 GHz with angular resolution sufficient to separate the source from the surrounding contaminating emission. Our increased sensitivity has allowed us to make unequivocal measurements of the variability of the linear polarization of this source in both position angle and polarization fraction. This is the first reliable detection of variation in the linear polarization fraction. Moreover, we have made the first detection of linear polarization changes within a night. These changes do not show an obvious correlation with the observed changes in the total intensity, possibly because of the coarse time resolution available at our sensitivity limits. The polarization variations occur on the shortest intervals we sample, around 3 hr, which is comparable to the modulation time observed in the total intensity here and in Mauerhan et al. (2005) at 100 GHz. It is not clear from these data whether the polarization variability can be best explained by changes in the source emission or by changes in an external Faraday screen, but polarization light curves with better time resolution should clarify the issue. The observed polarization fraction at 340 GHz is comparable to, and perhaps lower than, that observed at 230 GHz. This contradicts the polarization spectrum measured from 150 to 400 GHz by Aitken et al. (2000), but we show that their polarization fraction at 350 GHz can be brought into agreement with ours through changes in their correction for dust emission. Whether or not the polarization fraction rises steeply to high frequency, as predicted by synchrotron optical depth explanations of the early polarization results (Agol 2000; Melia et al. 2000), is no longer clear, but this question should be resolved by future submillimeter polarimetry at 650 GHz.

We have also measured the circular polarization of this source to be less than 0.5% for a time-stable component, and we do not detect CP at a slightly higher level in individual nights. This limit contradicts the predictions of the turbulence-driven polarization conversion model of Beckert (2003), which was designed to match the Aitken et al. (2000) linear polarization results, but can be matched to an earlier version of the model (Beckert & Falcke 2002) in which the CP originated in a fully turbulent jet.

By comparing the position angles in the two sidebands, we place new upper limits on the RM allowed for this source. In single nights we obtain 1 σ upper limits of less than 10^6 rad m^{-2}, with our lowest limit of 7×10^5 rad m^{-2} coming on July 5. This is comparable to the lowest limit obtained in any other polarimetric observations of this source and is well below the single-night limits of other interferometers. We can use a model accretion flow (with energy equipartition), parameterized only by the density power-law slope and the radius at which the electrons become relativistic, to convert this RM to a mass accretion rate limit, and we find that, for any density slope, Sgr A* is accreting at least an order of magnitude less matter than it should gravitationally capture on the basis of X-ray measurements (Baganoff et al. 2003) and may be accreting much less if the density profile is shallow. This result agrees with earlier interpretations of polarization detections. We note that the position angle at 340 GHz seems to show a persistent stable state, much like that observed at 230 GHz (Bower et al. 2005), and we combine these two values to infer a stable "quiescent" RM of -5×10^{-5} rad m^{-2}. This value is just below the detection limit of our observations. The possible proximity of the RM to the detection threshold, the need for more time-resolved polarimetry, and the potential for coordinated observations with other wavelengths suggests that expanded SMA capabilities may contribute considerably more to this study.

The authors thank the entire SMA team for their contributions to the array and to the new polarimetry system. In particular, we acknowledge the enormous contribution of K. Young for his work on the real-time software changes essential to these observations. We thank R. Narayan, E. Quataert, and G. Bower for useful discussions, and J. Greene for discussions and her help in developing the prototypes of the polarimetry system. D. P. M. was supported by an NSF Graduate Research Fellowship. We thank an anonymous referee for a thorough reading and helpful comments. Finally, we extend our gratitude to the Hawai'ian people, who allow us the privilege of observing from atop the sacred mountain of Mauna Kea.

REFERENCES

Agol, E. 2000, ApJ, 538, L121
Aitken, D. K., Greaves, J., Chrysostomou, A., Jenness, T., Holland, W., Hough, J. H., Pierce-Price, D., & Richer, J. 2000, ApJ, 534, L173
Baganoff, F. K., et al. 2001, Nature, 413, 45
———. 2003, ApJ, 591, 891
Beckert, T. 2003, Astron. Nachr. Suppl., 324, 459
Beckert, T., & Falcke, H. 2002, A&A, 388, 1106
Blandford, R. D., & Begelman, M. C. 1999, MNRAS, 303, L1
Blundell, R. 2004, in Proc. 15th International Symposium on Space Terahertz Technology, ed. G. Narayanan (Amherst: Univ. Massachusetts), 3, http://www.stt2004.org
Bondi, H. 1952, MNRAS, 112, 195
Bower, G. C., Falcke, H., & Backer, D. C. 1999a, ApJ, 523, L29
Bower, G. C., Falcke, H., Herrnstein, R. M., Zhao, J.-H., Goss, W. M., & Backer, D. C. 2004, Science, 304, 704
Bower, G. C., Falcke, H., Sault, R. J., & Backer, D. C. 2002, ApJ, 571, 843
Bower, G. C., Falcke, H., Wright, M. C., & Backer, D. C. 2005, ApJ, 618, L29
Bower, G. C., Wright, M. C. H., Backer, D. C., & Falcke, H. 1999b, ApJ, 527, 851
Bower, G. C., Wright, M. C. H., Falcke, H., & Backer, D. C. 2001, ApJ, 555, L103
———. 2003, ApJ, 588, 331
Cuadra, J., Nayakshin, S., Springel, V., & Di Matteo, T. 2006, MNRAS, 366, 358
Dowell, C. D., et al. 2003, Proc. SPIE, 4855, 73
Eckart, A., et al. 2004, A&A, 427, 1
———. 2006, A&A, in press (astro-ph/0512440)
Eisenhauer, F., et al. 2005, ApJ, 628, 246
Falcke, H., Mannheim, K., & Biermann, P. L. 1993, A&A, 278, L1
Gardner, F. F., & Whiteoak, J. B. 1966, ARA&A, 4, 245
Genzel, R., Schödel, R., Ott, T., Eckart, A., Alexander, T., Lacombe, F., Rouan, D., & Aschenbach, B. 2003, Nature, 425, 934
Ghez, A. M., Salim, S., Hornstein, S. D., Tanner, A., Lu, J. R., Morris, M., Becklin, E. E., & Duchêne, G. 2005, ApJ, 620, 744
Ho, P. T. P., Moran, J. M., & Lo, K. Y. 2004, ApJ, 616, L1
Holland, W. S., et al. 1999, MNRAS, 303, 659
Krichbaum, T. P., et al. 1998, A&A, 335, L106
Markoff, S., Falcke, H., Yuan, F., & Biermann, P. L. 2001, A&A, 379, L13
Mauerhan, J. C., Morris, M., Walter, F., & Baganoff, F. K. 2005, ApJ, 623, L25
Melia, F. 1992, ApJ, 387, L25
Melia, F., Liu, S., & Coker, R. 2000, ApJ, 545, L117
Miyazaki, A., Tsutsumi, T., & Tsuboi, M. 2004, ApJ, 611, L97
Narayan, R., & Yi, I. 1994, ApJ, 428, L13
———. 1995, ApJ, 452, 710

Pen, U.-L., Matzner, C. D., & Wong, S. 2003, ApJ, 596, L207
Pierce-Price, D., et al. 2000, ApJ, 545, L121
Quataert, E. 2003, Astron. Nachr. Suppl., 324, 435
———. 2004, ApJ, 613, 322
Quataert, E., & Gruzinov, A. 2000a, ApJ, 539, 809
———. 2000b, ApJ, 545, 842
Rao, R. P. 1999, Ph.D. thesis, Univ. Illinois, Urbana-Champaign
Reid, M. J., & Brunthaler, A. 2004, ApJ, 616, 872
Roberts, D. H., Wardle, J. F. C., & Brown, L. F. 1994, ApJ, 427, 718
Sault, R. J., Hamaker, J. P., & Bregman, J. D. 1996, A&AS, 117, 149
Sault, R. J., & Macquart, J.-P. 1999, ApJ, 526, L85
Sault, R. J., Teuben, P. J., & Wright, M. C. H. 1995, in ASP Conf. Ser. 77, Astronomical Data Analysis Software and Systems IV, ed. R. A. Shaw, H. E. Payne, & J. J. E. Hayes (San Francisco: ASP), 433
Schödel, R., Ott, T., Genzel, R., Eckart, A., Mouawad, N., & Alexander, T. 2003, ApJ, 596, 1015
Serabyn, E., Carlstrom, J., Lay, O., Lis, D. C., Hunter, T. R., & Lacy, J. H. 1997, ApJ, 490, L77
Shen, Z.-Q., Lo, K. Y., Liang, M.-C., Ho, P. T. P., & Zhao, J.-H. 2005, Nature, 438, 62
Tribble, P. C. 1991, MNRAS, 250, 726
Tsuboi, M., Miyahara, H., Nomura, R., Kasuga, T., & Miyazaki, A. 2003, Astron. Nachr. Suppl., 324, 431
Wardle, J. F. C., & Kronberg, P. P. 1974, ApJ, 194, 249
Yuan, F., Quataert, E., & Narayan, R. 2003, ApJ, 598, 301
Zylka, R., Mezger, P. G., Ward-Thompson, D., Duschl, W. J., & Lesch, H. 1995, A&A, 297, 83